THE JOURNAL OF PHYSICAL CHEMISTRY C

pubs.acs.org/JPCC Article

Impact of Magnetic Field Strength on Resolution and Sensitivity of Proton Resonances in Biological Solids

Kai Xue, Riddhiman Sarkar,* Daniela Lalli, Benita Koch, Guido Pintacuda, Zdenek Tosner, and Bernd Reif*

Cite This: https://dx.doi.org/10.1021/acs.jpcc.0c05407 Read Online

ACCESS | Metrics & More | Article Recommendations | Supporting Information

ABSTRACT: Sensitivity and resolution together determine the quality of NMR spectra in biological solids. Higher magic angle spinning frequencies yield a more efficient suppression of the coupling network and enable atomic-level investigations of protonated protein samples. On the other hand, truncation effects induced by higher magnetic fields have an impact on the achievable sensitivity and resolution. In this work, we address the question of how the proton dipolar coupling network affects the magnetic field strength-dependent gains in sensitivity and resolution. We find that—beyond the canonical $B_0^{3/2}$ dependence—an additional factor of 2 in sensitivity can be achieved for residues embedded in the core of the protein, when the static magnetic field induces a transition from the strong- to the weak-coupling limit. The experiments are carried out using a selectively methyl-protonated (^{13}CH3) α-spectrin SH3 sample, at magnetic field strengths of 11.75 T (^{1}H Larmor frequency of 500 MHz) and 23.5 T (^{1}H Larmor frequency of 1 GHz).

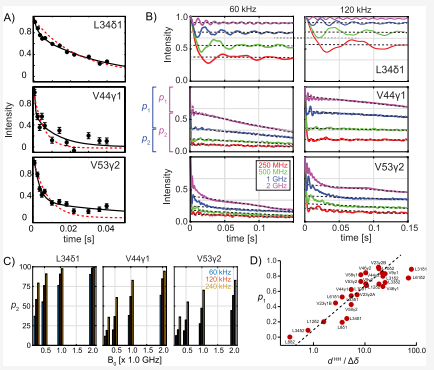

INTRODUCTION

Structure determination of protonated proteins using proton-detected solid-state NMR experiments, acquired at high magnetic fields (1 GHz) and fast (100 kHz) magic angle spinning (MAS), was first demonstrated in 2016.[1] Since then, fast MAS has revolutionized biological solid-state NMR.[2−7] Fast sample spinning at the magic angle is a prerequisite for proton-detected high-resolution solid-state NMR.[8] Faster sample spinning averages anisotropic interactions more efficiently, which results in better sensitivity in correlation spectra.[9] The effect of the MAS rotation frequency on the resolution of amide and methyl proton spectra has been studied recently.[8,10−12] It has been shown that T_2' of amide protons increases proportionally with the inverse of the rotor period for most residues in a model protein.[13] As the effective dipole−dipole interaction experienced by methyl protons is much larger than that for any other type of protons in a protein, methyl protons yield the largest line widths, even though the intramethyl dipolar couplings are scaled because of the fast rotation of the methyl group.[14] For a selectively methyl-protonated sample in an otherwise deuterated background, MAS frequencies above 300 kHz are necessary to yield 80% of the maximum attainable signal intensity.[11] For MAS frequencies below 70 kHz, $^{13}CHD_2$ methyl group labeling is necessary to obtain optimal spectral quality. Above an MAS frequency of 70 kHz, $^{13}CH_3$ isotopomers[4,15−17] yield the best sensitivity depending on the density of the proton spin system.[12]

The maximum achievable rotation frequency of an MAS rotor is limited by the speed of sound on the rotor surface.[18] Higher rotation frequencies can therefore only be obtained for ever smaller diameter rotors. Lower sample mass is thus traded for faster MAS rates. At first sight, this seems to come at the cost of sensitivity. A 0.7 mm MAS rotor that spins as fast as 110 kHz accommodates effectively less than a milligram of the sample.[19] As the length of an MAS rotor scales approximately linearly with its diameter, the amount of sample in a fast spinning rotor decreases proportionally with r.[3] On the other hand, the quality factor of the coil and the efficiency of detection increase with smaller coil diameters proportional to $1/r$.[20] The apparent coherence decay time T_2' and thus the signal intensity during proton detection increase with higher MAS frequencies. Longer T_2' times contribute to the overall intensity linearly with $1/r$.[8,13,21] Even though the Hartmann−Hahn matching conditions become more selective at high MAS rotation frequencies,[22,23] ^{1}H−T_2' and $T_{1\rho}$ relaxation times increase at faster MAS frequencies which facilitate multidimensional solid-state NMR experiments with multiple magnetization transfer steps.[7] Assuming that polarization transfer contributes another factor proportional to $1/r$ to the

Received: June 15, 2020
Revised: September 21, 2020

relative signal intensity, comparable sensitivities, for example, 1.3 and 0.7 mm samples, are expected. This, in fact, has been observed experimentally.[1] When the MAS frequency is large enough to efficiently average proton−proton dipolar couplings such that ^{1}H transversal relaxation times do not any longer increase linearly with the rotation frequency, the optimum gain in the signal to noise ratio (SNR) is reached. For selectively methyl-protonated protein samples, this break-even point occurs for MAS frequencies on the order of 300 kHz.[11] For protonated samples, presumably higher MAS rotation frequencies are needed.

Obviously, proton sensitivity is not influenced by the employed MAS frequency alone. The detection sensitivity depends on the external magnetic field strength and is proportional to $B_0^{3/2}$.[20,24] The experimental gain depends on a number of parameters including the conductivity of the sample and hardware parameters such as probe design, preamplifier, and receiver electronics. It is therefore not the aim of the manuscript to quantify the absolute field-dependent gain in sensitivity. We rather focus on the site-specific sensitivity ratios which are determined by the local geometry of the sample and the chemical shift differences among the coupled methyl groups. Even larger gains in sensitivity and resolution are expected in case proton−proton dipolar interactions transition from a strong coupling into a weak coupling limit with increasing magnetic field strength. This transition should occur when the chemical shift difference between interacting protons exceeds the strength of the involved effective dipolar coupling. In this manuscript, we explore the field-dependent relative site-specific gain in the sensitivity of proton-detected ^{1}H, ^{13}C correlation spectra obtained for selectively methyl protonated microcrystalline protein samples. We find that, in particular, methyl groups that are located in proton dense regions yield gains in sensitivity that exceed the expected factor of 2.83, in case experiments are recorded at 24.2 T (1 GHz) instead of 12.1 T (500 MHz). These additional gains can be as large as an additional factor of 2 and depend on the local spin density and the chemical shift between interacting protons.

RESULTS

This study was motivated by the observation that ^{1}H, ^{13}C correlation spectra that were recorded using protonated microcrystalline proteins at an MAS frequency of 106 kHz are significantly better resolved at 1 GHz in comparison to 500 MHz (Figure 1;[14]). This applies, in particular, to the methyl region of the spectra. At the same time, the Cα region seems less affected. We explained this difference previously by considering the significantly higher effective dipolar couplings experienced by methyl protons compared to Cα bound protons.[14,25] However, the significant difference in resolution of the methyl region at the two magnetic fields raised the question on the field dependence of the proton line width.

Figure 2A shows ^{1}H, ^{13}C correlation spectra of a selectively $^{13}CH_3$ methyl-protonated SH3 sample recorded at 500 MHz (left) and 1 GHz (right). The spectra were acquired at an MAS frequency of 90 kHz. The site-specific SNRs for each methyl group are represented in Figure 2B. The spectrum recorded at 1 GHz shows a significantly higher SNR (on average, 2.1 times higher) for all methyl groups. To find out whether sensitivity improves beyond the theoretically expected factor, we calculated a theoretical SNR value for 1 GHz from the experimental sensitivity at 500 MHz using the following equation

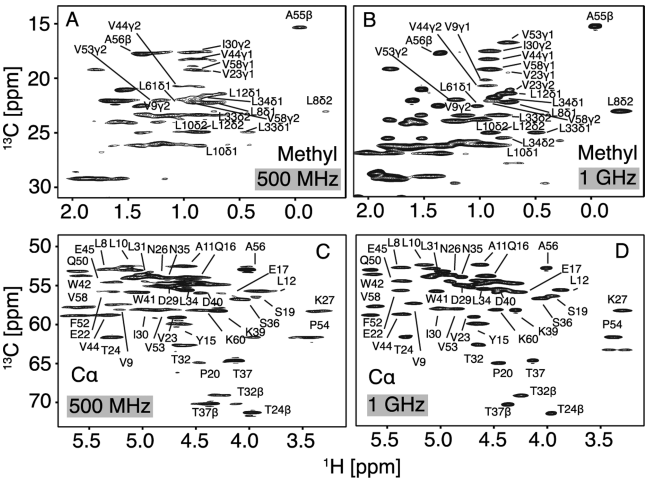

Figure 1. ^{1}H, ^{13}C correlation spectra of a fully protonated u-[^{13}C, ^{15}N] microcrystalline αSH3 domain recorded at an MAS frequency of 106 kHz and at magnetic fields of 11.75 T (A,C) and 23.5 T (B,D), respectively. Methyl (top) and Cα regions (bottom) of the spectra are shown. Representative 1D traces of spectra are shown in Figure S6.

$$\mathrm{SNR}_{1\mathrm{GHz}} = \mathrm{SNR}_{500\mathrm{MHz}} \times \left(\frac{\mathrm{LW(C)}_{500\mathrm{MHz}} \times \mathrm{LW(H)}_{500\mathrm{MHz}}}{\mathrm{LW(C)}_{1\mathrm{GHz}} \times \mathrm{LW(H)}_{1\mathrm{GHz}}}\right) \times \left(\frac{\epsilon_{1GHz}}{\epsilon_{500MHz}}\right) \times \left(\frac{1000}{500}\right)^{3/2} \quad (1)$$

where LW $(\chi)_\psi$ represents the line width of nucleus χ at a B_0 field of ψ; ε_ψ corresponds to the transfer efficiency after two CP steps in the ^{1}H, ^{13}C correlation experiments as $\varepsilon_\psi = \varepsilon(\mathrm{H} \rightarrow \mathrm{C}) \times \varepsilon(\mathrm{C} \rightarrow \mathrm{H})$. As shown in Figure 2C, the site-specific CP efficiencies are slightly larger at 1 GHz than at 500 MHz. ε_ψ is measured by comparing the cross-peak intensities of ^{1}H, ^{13}C correlation spectra that involve four versus two CP steps,[26] as described in Figure S3. The ^{1}H and ^{13}C line widths at 1 GHz are slightly larger (mean: 68.9 Hz for ^{1}H and 21.4 Hz for ^{13}C) compared to 500 MHz (mean: 61.1 Hz for ^{1}H and 14.8 Hz for ^{13}C), as seen from Figures 2D and S4. Larger line widths at 1 GHz can potentially be attributed to crystal heterogeneity, shimming, and the anisotropy of the bulk magnetic susceptibility (ABMS). Because of the increased magnetic fields, the SNR should improve ~2.8-fold [$=(1000/500)^{3/2}$] theoretically.

Figure 3B shows the experimental site-specific SNR at 1 GHz versus the SNR calculated from eq 1. Residues such as L33, L34 (δ1 and δ2), L10 (δ1 and δ2), and V44 (γ1 and γ2) show a good agreement between experimental and predicted intensities as they are located close to the diagonal. For residues such as V9, V23, and V53 (inset to Figure 3B), the additional experimental gains can be as large as 2. To explain this unusual gain in the SNR at higher B_0 fields, we inspected the ^{1}H line shapes more carefully (Figure 3A). The ^{1}H resonances of most of the residues feature a broad and a narrow component. In the figure, the broad component is indicated with a red arrow. This is in agreement with simulations that have predicted these spectral patterns previously (Xue et al., 2018, Figures S3−S5). As the broad

https://dx.doi.org/10.1021/acs.jpcc.0c05407
J. Phys. Chem. C XXXX, XXX, XXX−XXX

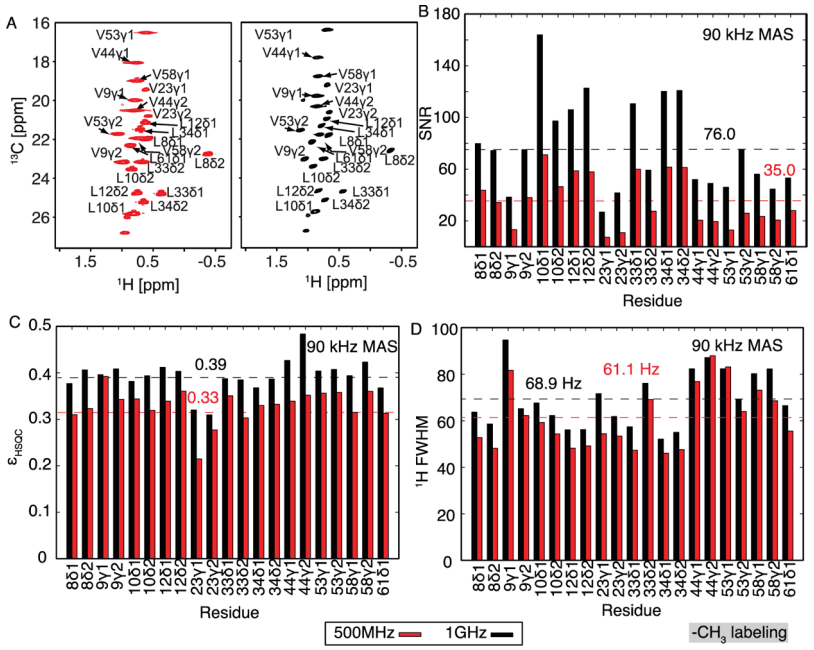

Figure 2. (A) ^{1}H, ^{13}C correlation spectra recorded at an MAS frequency of 90 kHz for a selectively valine and leucine methyl-protonated αSH3 domain sample. Except for the methyl groups, the protein is fully deuterated, including the exchangeable sites. Measurements were performed at B_0 fields of 500 MHz (red) and 1 GHz (black). (B) SNR of the cross peaks increases from a mean of 35:1 to 76:1 when the field is increased from 500 MHz to 1 GHz. (C) Site-specific polarization transfer efficiencies $\varepsilon_{HCH} = \varepsilon(H \rightarrow C) \times \varepsilon(C \rightarrow H)$ for Hartmann−Hahn-based cross polarization transfers at 500 MHz and 1 GHz. The transfer efficiencies are slightly higher at 1 GHz in comparison to 500 MHz. (D) Proton line width as a function of residue. The mean line width (fwhm) for spectra recorded at 1 GHz is slightly larger compared to the line width obtained from spectra recorded at 500 MHz.

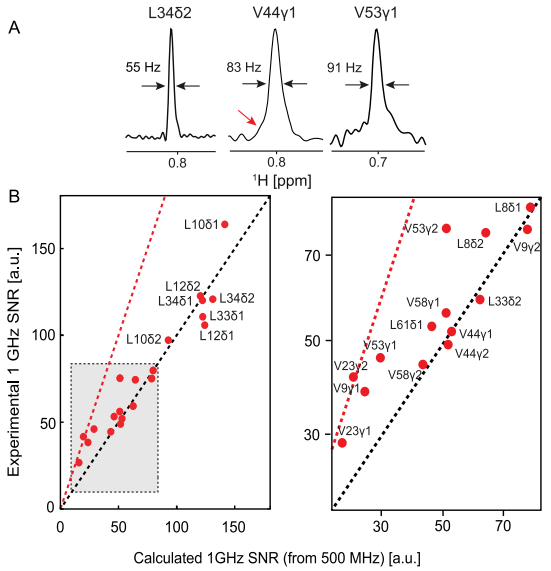

Figure 3. Traces extracted along the proton dimension ^{1}H, ^{13}C correlation spectra from Figure 2A (1 GHz) for the methyl cross peaks L34δ2, V44γ1, and V53γ1 for a selectively valine and leucine methyl-protonated αSH3 domain sample. (B) Correlation of the experimental intensity at 1 GHz (vertical axis) and the predicted intensity (horizontal axis) using intensity values obtained at 500 MHz and eq 1. For peaks with relatively high intensity, a good correlation is observed (black, dashed line at $y = x$). For peaks with relatively low intensity, however, the experimental intensities at 1 GHz are significantly higher than those expected from the 500 MHz data (shaded region; magnified in the right-hand side panel, red, dashed line at $y = 2 \times x$).

component is difficult to appreciate in Fourier transformed NMR spectra, we turned to the analysis of T_2' echo decays (Figure 4). We find experimentally that the apparent site-specific ^{1}H transverse relaxation (T_2') decays with a multi-exponential behavior (Figure 4A). Fast methyl group rotation contributes an incoherent component to the ^{1}H−T_2' decay. On the other hand, Simpson simulations that consider only coherent ^{1}H, ^{1}H dipolar interactions suggest that magnetization decays at least biexponentially, as described previously in ref 11. We therefore empirically describe the decay of ^{1}H transverse magnetization (T_2') using the following equation

$$S(t) = p_0 \times \exp\left(-\frac{t}{T_2^{inc}}\right) + p_1 \times \exp\left(-\frac{t}{T_2^{coh,fast}}\right) + p_2 \times \exp\left(-\frac{t}{T_2^{coh,slow}}\right) \quad (2)$$

with $p_0 + p_1 + p_2 = 1$.

In eq 2, the component proportional to p_0 refers to relaxation due to an incoherent mechanism with a characteristic time constant T_2^{inc}. p_1 and p_2 refer to the signal components that are due to coherent dephasing of magnetization and that decay with the characteristic time constants $T_2^{coh,fast}$ and $T_2^{coh,slow}$, respectively.

To appreciate the multiexponential magnetization decay due to coherent effects, we performed Simpson simulations.[27,28] In the simulation, a spin system involving nine spins is assumed using the PDB coordinate file of the α-spectrin SH3 X-ray structure (PDB ID: 2NUZ).[29] Chemical shift data were taken from Asami et al.[30] The simulations were performed as functions of the B_0 field and for several MAS frequencies. Figure 4B shows the simulated ^{1}H−T_2' decay curves for L34δ1,

https://dx.doi.org/10.1021/acs.jpcc.0c05407
J. Phys. Chem. C XXXX, XXX, XXX−XXX

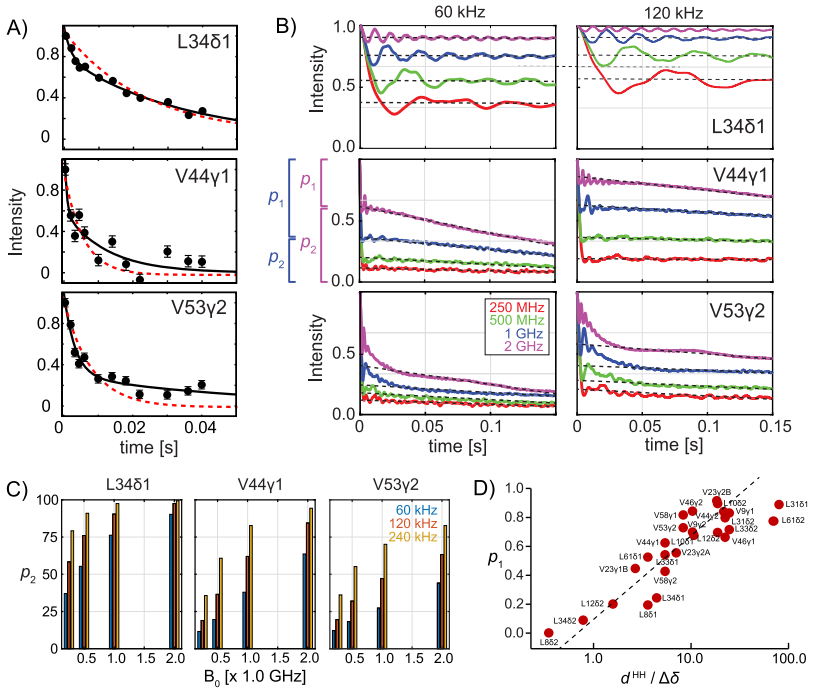

Figure 4. (A) Experimental $^{1}H-T_2'$ decay curves (recorded by employing 90 kHz MAS at a B_0 field of 1 GHz) for a few representative residues in the microcrystalline selectively CH3-protonated αSH3 sample. Multiexponential fits are required to adequately describe the experimental data. (B) Simpson simulations of ^{1}H Hahn echo experiments for L34δ1, V44γ1, and V53γ2, assuming exact geometry of the αSH3 domain. For the simulations, nine proton spins have been taken into account. The parameters p_1 and p_2 are employed to empirically describe the simulations. (C) Slowly decaying component p_2 is shown as a function of B_0 and MAS frequency. (D) Correlation of p_1 and $d^{HH}/\Delta\delta$ (ratio of proton−proton dipolar coupling to the chemical shift difference of the strongest coupling partner), assuming a magnetic field strength of 1 GHz.

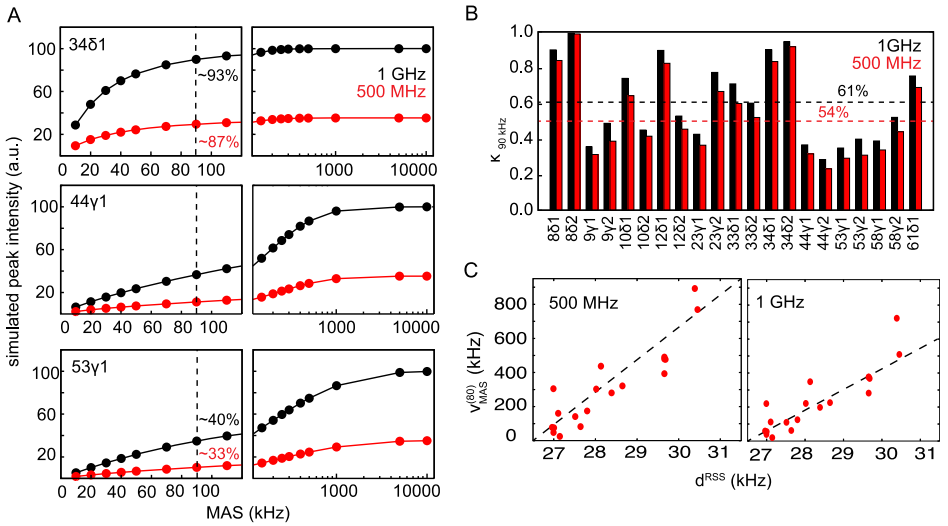

Figure 5. (A) Simulated intensities for methyl protons of L34δ2, V44γ1, and V53γ1 calculated by assuming B_0 fields of 500 MHz and 1 GHz and assuming that only valine and leucine methyl groups are labeled $^{13}CH_3$ (while rest of the protein is deuterated) for the αSH3 domain sample. At an MAS frequency of 90 kHz, a systematically higher SNR is expected for 1 GHz compared to 500 MHz. The percent numbers in the figure (κ_{90kHz}) indicate the fraction of the maximum achievable sensitivity obtained at an MAS frequency of 90 kHz. (B) κ_{90kHz} for each methyl group in α-SH3 calculated for magnetic field strengths of 500 MHz (red) and 1 GHz (black). (C) Correlation of the characteristic MAS frequency necessary to obtain 80% of the maximum achievable intensity $\nu_{MAS}^{(80)}$ vs the effective dipolar coupling d^{RSS} at 500 MHz (left) and 1 GHz (right). The slope of the correlation plot decreases for higher fields, suggesting that high fields facilitate line narrowing by MAS.

V44γ1, and V53γ2 at MAS rotation frequencies of 60 and 120 kHz and for static magnetic fields of 250 MHz, 500 MHz, 1 G Hz, and 2 GHz. All simulations show that magnetization declines much more slowly after an initial very fast decay. The associated intensity fractions are referred to as p_1 and p_2, respectively.

The B_0 dependence of the slowly decaying component p_2 is shown in Figure 4C. Because of higher chemical shift dispersion, the contribution of the slowly decaying component to the spin echo signal increases when the static magnetic field B_0 is increased. For V53γ2, p_2 increases from 0.19 to 0.64 while going from 250 MHz to 2 GHz at a fixed MAS frequency of

https://dx.doi.org/10.1021/acs.jpcc.0c05407
J. Phys. Chem. C XXXX, XXX, XXX−XXX

120 kHz. Faster MAS facilitates averaging of proton−proton dipolar interactions. As a consequence, an MAS frequency of 240 kHz yields a p_2 value of 0.55 even at a static field of 500 MHz, while p_2 is as low as 0.27 at an MAS frequency of 60 kHz at a static B_0 field of 1 GHz. L34δ2 is a methyl group that is only weakly coupled with other protons. As a consequence, p_2 reaches a value of 0.9 at an MAS frequency and B_0 field of 120 kHz and 1 GHz, respectively.

In order to find out how the fast decaying component correlates with the effective proton−proton dipolar coupling and the chemical shift difference to the strongest coupling partner, defined as $d^{HH}/\Delta\delta$, we have represented p_1 as a function of $d^{HH}/\Delta\delta$ (Figure 4D). In the simulation, a static magnetic field B_0 of 1 GHz is assumed. p_1 correlates well with $d^{HH}/\Delta\delta$. For $d^{HH}/\Delta\delta < 1$, we in fact find that the fast decaying component vanishes. As an example, V53γ2 is densely packed in the core of α-SH3. The nearest residue V58γ1 exhibits a dipolar coupling of $d^{HH}/2\pi \sim 2392$ Hz, while $\Delta\delta \sim 288$ Hz at 1 GHz. The spin echo decay for V53γ2 yields a significantly higher $p_1 \sim 0.7$ compared to L34δ2, for which $d^{HH}/\Delta\delta$ is small ($p_1 \sim 0.08$; $d^{HH}/2\pi \sim 237$ Hz, while $\Delta\delta \sim 303$ Hz at 1 GHz).

f5 Figure 5A shows the simulated signal intensities as a function of B_0 and the MAS frequency for a few representative residues. Obviously, higher intensities are obtained at higher magnetic field strengths. In order to appreciate how the intensity of a particular methyl group relates to the maximum possible sensitivity, we introduce the parameter κ_{90kHz}. κ_{90kHz} refers to the fraction of the maximum achievable sensitivity (where simulated intensity reaches a plateau) obtained at an MAS frequency of 90 kHz. For V53γ2, κ_{90kHz} amounts to ∼33% at 500 MHz, while this value increases to $\kappa_{90kHz} \sim 40\%$ at a field of 1 GHz. Similarly, κ_{90kHz} is equal to 87 and 93% for L34δ2 at B_0 fields of 500 MHz and 1 GHz, respectively. On average, κ_{90kHz} is on the order of ∼54% at a B_0 of 500 MHz, while κ_{90kHz} increases to ∼61% at a B_0 field of 1 GHz (Figure 5B). This indicates that high magnetic fields imply gains in sensitivity that are beyond the canonical ${B_0}^{3/2}$ dependence. Figure 5C shows a correlation between the characteristic MAS frequency $\nu^{(80)}_{MAS}$ and the effective dipolar coupling d^{RSS} for α-SH3 (where d^{RSS} is defined as $d_i^{RSS} = \frac{\mu_0}{4\pi}\gamma_H^2\sqrt{\sum_j\left(\frac{1}{r_{i,j}^3}\right)^2}$). The characteristic MAS frequency is defined as the frequency which is required to obtain 80% of the maximum intensity for a given residue. Again, higher magnetic fields facilitate MAS-induced averaging of proton dipolar couplings.[11,12]

CONCLUSIONS

In this work, we have compared the site-specific increase in sensitivity for methyl protons in a microcrystalline, selectively methyl-protonated α-spectrin SH3 domain sample, implied by the increase in the external magnetic B_0 field from 500 MHz to 1 GHz by employing fast MAS (90 kHz). For residues that experience few proton−proton dipolar interactions, the increase in sensitivity closely matches the expected value of ∼2.1, as described by eq 1. However, the gain in SNR can be increased by an additional factor of ∼2 for methyls that are embedded in a dense proton coupling network such as V9γ1, V23γ2, and V53γ1. These additional gains can be explained by a decreased dipolar coupling to chemical shift difference ratio ($d^{HH}/\Delta\delta$), inducing a transition into the weak coupling limit. We find that the proton line shapes feature a broad and a narrow component. Using numerical simulations, we could show that the broad component contributes less at higher B_0 fields. Our results indicate that fast MAS in combination with high B_0 fields is essential to yield proton spectra with optimum sensitivity and resolution in the solid state. It is expected that modifying the proton network in the sample by protonation of the amide groups or the side chains may impact the site-specific intensity gains.[17]

MATERIALS AND METHODS

Sample Preparation. The microcrystalline, perdeuterated, and selectively methyl-protonated SH3 domain sample was prepared as described previously.[31] In brief, expression was carried out in a 100% D_2O M9 medium, supplemented with ^{15}N-ammonium chloride and u-[^{2}H, ^{13}C]-D-glucose. α-Ketoisovalerate (2-keto-3-(methyl-d_3)-butyric acid-4-^{13}C sodium salt, Sigma-Aldrich) was added to the M9 medium 1 h prior to induction with 1 mM IPTG (at OD_{600} 0.5−0.6), yielding a 50% incorporation rate of CH3 isotopomers in either the pro-R or pro-S position of the valine and leucine side chains. Subsequent to overnight expression, the SH3 domain was purified via anion exchange and size exclusion chromatography. For crystallization, pure protein was lyophilized and dissolved in 100% D_2O (final concentration: 8−10 mg/mL). Ammonium sulfate (dissolved in 100% D_2O) was added to a final concentration of 100 mM, and the pH was adjusted to 8.0 by adding NaOD. The protonated sample was prepared by employing only protonated chemicals.

Solid-State NMR. NMR experiments were carried out at B_0 fields of 500 MHz and 1 GHz by employing a 0.7 mm H/C/N triple-resonance MAS probe. As the sample was recrystallized from 100% D_2O, no solvent suppression was employed. For all experiments, the sample temperature was adjusted to the same effective value using DSS and the residual water signal for calibration. The pulse sequences used to quantify the transfer efficiency are reported in the Supporting Information (Figure S3). The following matching conditions were employed at a B_0 field of 1 GHz: $\omega_1(^{13}C)/2\pi = 60$ kHz and $\omega_1(^1H)/2\pi = 177$ kHz at an MAS frequency of 106 kHz and $\omega_1(^{13}C)/2\pi = 60$ kHz and $\omega_1(^1H)/2\pi = 160$ kHz at an MAS frequency of 90 kHz. In all cases, a 90−100 ramped shape was used on the ^{1}H channel, whereas a constant amplitude pulse was used for ^{13}C. For experiments carried out at 500 MHz, the following matching conditions were employed: $\omega_1(^{13}C)/2\pi = 40$ kHz and $\omega_1(^1H)/2\pi = 70$ kHz at an MAS frequency of 106 kHz and $\omega_1(^{13}C)/2\pi = 40$ kHz and $\omega_1(^1H)/2\pi = 50$ kHz at an MAS frequency of 90 kHz. In all cases, a 70−100 ramped shape was used on the ^{1}H channel, whereas a constant amplitude pulse was used for ^{13}C. The contact times for the transfers $^1H \rightarrow {}^{13}C$ and $^{13}C \rightarrow {}^1H$ were set to 500 μs for both samples. The relaxation delay was set to 1 and 0.63 s in 1 GHz and 500 MHz, respectively, which is about 1.5 times the experimentally determined bulk proton T1 (Figure S7). The error in signal intensities introduced by relaxation is estimated to be less than 10%. The acquisition times were set to 20 and 70 ms in ^{1}H and ^{13}C dimensions, respectively. Proton line widths were compared to experiments recorded by employing an acquisition time of 50 ms, which showed no gain in resolution. Signals were not apodized when line widths were compared. Of note, the same rotor was used for all the experiments in both the spectrometers.

Numerical Simulations. The numerical simulations were carried out using a nine-proton spin system, thus accounting for two neighboring methyl-containing side chains. Because the

https://dx.doi.org/10.1021/acs.jpcc.0c05407
J. Phys. Chem. C XXXX, XXX, XXX−XXX

incorporation of $^{13}CH_3$ and $^{12}CD_3$ into the pro-R and pro-S positions occurs at random, selecting the two closest neighboring methyl groups for a given site overestimates the involved dipole−dipole couplings. Using the program SIMPSON, we have therefore calculated the methyl proton spectra for all permutations to reflect the actual isotope labeling of the sample. Subsequently, the average spectrum has been calculated. For the spin echo simulations, two closest methyl groups were chosen for a given methyl group; the gcompute method in the time domain was used with block diagonalization of Hamiltonians whenever possible. Long echo delays were simulated using a precalculated propagator of one rotor period which was raised to the exponent as necessary.

■ ASSOCIATED CONTENT

Supporting Information

The Supporting Information is available free of charge at https://pubs.acs.org/doi/10.1021/acs.jpcc.0c05407.

Site specific intensities and proton line shapes, pulse sequences to record ^1H, ^{13}C spectra and Hartmann−Hahn CP efficiencies, experimental ^{13}C line widths, site-specific apparent ^1H T_2' decay curves, 1D traces from correlation spectra, and bulk ^1H T_1 curves at 500 MHz and 1 GHz (PDF)

■ AUTHOR INFORMATION

Corresponding Authors

Riddhiman Sarkar − *Helmholtz-Zentrum München (HMGU), Deutsches Forschungszentrum für Gesundheit und Umwelt, 85764 Neuherberg, Germany; Munich Center for Integrated Protein Science (CIPS-M) at Department Chemie, Technische Universität München (TUM), 85747 Garching, Germany;* orcid.org/0000-0001-9055-7897; Email: riddhiman.sarkar@helmholtz-muenchen.de

Bernd Reif − *Helmholtz-Zentrum München (HMGU), Deutsches Forschungszentrum für Gesundheit und Umwelt, 85764 Neuherberg, Germany; Munich Center for Integrated Protein Science (CIPS-M) at Department Chemie, Technische Universität München (TUM), 85747 Garching, Germany;* orcid.org/0000-0001-7368-7198; Email: reif@tum.de

Authors

Kai Xue − *Helmholtz-Zentrum München (HMGU), Deutsches Forschungszentrum für Gesundheit und Umwelt, 85764 Neuherberg, Germany*

Daniela Lalli − *Centre de Résonance Magnétique Nucléaire a Très hauts Champs (FRE 2034-CNRS, Ecole Normale Supérieure de Lyon, Université Claude Bernard Lyon 1), Université de Lyon, 69100 Villeurbanne, France*

Benita Koch − *Munich Center for Integrated Protein Science (CIPS-M) at Department Chemie, Technische Universität München (TUM), 85747 Garching, Germany*

Guido Pintacuda − *Centre de Résonance Magnétique Nucléaire a Très hauts Champs (FRE 2034-CNRS, Ecole Normale Supérieure de Lyon, Université Claude Bernard Lyon 1), Université de Lyon, 69100 Villeurbanne, France;* orcid.org/0000-0001-7757-2144

Zdenek Tosner − *Department of Chemistry, Faculty of Science, Charles University, 12842 Praha 2, Czech Republic*

Complete contact information is available at: https://pubs.acs.org/10.1021/acs.jpcc.0c05407

Notes

The authors declare no competing financial interest.

■ ACKNOWLEDGMENTS

This work was performed in the framework of the SFB-1035 (project B07; German Research Foundation, DFG). We acknowledge support from the Helmholtz-Gemeinschaft, the Deutsche Forschungsgemeinschaft (DFG, Grant Re1435), the Center for Integrated Protein Science Munich (CIPS-M), the CNRS (IR-RMN FR3050), the Czech Science Foundation (grant no. 20-00166J (Z.T.)), the European Research Council (ERC) (ERC-2014-CoG "P-MEM-NMR" GA n 648974), and the EU access project iNext (GA 653706). Computational resources were supplied by the project "e-Infrastruktura CZ" (e-INFRA LM2018140) provided within the program Projects of Large Research, Development and Innovations Infrastructures.

■ REFERENCES

(1) Andreas, L. B.; Jaudzems, K.; Stanek, J.; Lalli, D.; Bertarello, A.; Le Marchand, T.; Cala-De Paepe, D.; Kotelovica, S.; Akopjana, I.; Knott, B.; et al. Structure of fully protonated proteins by proton-detected magic-angle spinning NMR. *Proc. Natl. Acad. Sci. U.S.A.* **2016**, *113*, 9187−9192.

(2) Stanek, J.; Andreas, L. B.; Jaudzems, K.; Cala, D.; Lalli, D.; Bertarello, A.; Schubeis, T.; Akopjana, I.; Kotelovica, S.; Tars, K.; et al. NMR Spectroscopic Assignment of Backbone and Side-Chain Protons in Fully Protonated Proteins: Microcrystals, Sedimented Assemblies, and Amyloid Fibrils. *Angew. Chem., Int. Ed.* **2016**, *55*, 15503−15509.

(3) Vasa, S. K.; Singh, H.; Grohe, K.; Linser, R. Assessment of a Large Enzyme-Drug Complex by Proton-Detected Solid-State NMR Spectroscopy without Deuteration. *Angew. Chem., Int. Ed.* **2019**, *58*, 5758−5762.

(4) Gauto, D. F.; Estrozi, L. F.; Schwieters, C. D.; Effantin, G.; Macek, P.; Sounier, R.; Sivertsen, A. C.; Schmidt, E.; Kerfah, R.; Mas, G.; et al. Integrated NMR and cryo-EM atomic-resolution structure determination of a half-megadalton enzyme complex. *Nat. Commun.* **2019**, *10*, 2697.

(5) Gauto, D. F.; Macek, P.; Barducci, A.; Fraga, H.; Hessel, A.; Terauchi, T.; Gajan, D.; Miyanoiri, Y.; Boisbouvier, J.; Lichtenecker, R.; et al. Aromatic Ring Dynamics, Thermal Activation, and Transient Conformations of a 468 kDa Enzyme by Specific 1H−13C Labeling and Fast Magic-Angle Spinning NMR. *J. Am. Chem. Soc.* **2019**, *141*, 11183−11195.

(6) Kosol, S.; Gallo, A.; Griffiths, D.; Valentic, T. R.; Masschelein, J.; Jenner, M.; de los Santos, E. L. C.; Manzi, L.; Sydor, P. K.; Rea, D.; et al. Structural basis for chain release from the enacyloxin polyketide synthase. *Nat. Chem.* **2019**, *11*, 913−923.

(7) Orton, H. W.; Stanek, J.; Schubeis, T.; Foucaudeau, D.; Ollier, C.; Draney, A. W.; Le Marchand, T.; Cala-De Paepe, D.; Felli, I. C.; Pierattelli, R.; et al. Protein NMR Resonance Assignment without Spectral Analysis: 5D SOlid-State Automated Projection SpectroscopY (SO-APSY). *Angew. Chem., Int. Ed.* **2020**, *59*, 2380−2384.

(8) Samoson, A.; Tuherm, T.; Gan, Z. High-Field High-Speed MAS Resolution Enhancement in 1H NMR Spectroscopy of Solids. *Solid State Nucl. Magn. Reson.* **2001**, *20*, 130−136.

(9) Böckmann, A.; Ernst, M.; Meier, B. H. Spinning proteins, the faster, the better? *J. Magn. Reson.* **2015**, *253*, 71−79.

(10) Malär, A. A.; Smith-Penzel, S.; Camenisch, G.-M.; Wiegand, T.; Samoson, A.; Böckmann, A.; Ernst, M.; Meier, B. H. Quantifying proton NMR coherent linewidth in proteins under fast MAS conditions: a second moment approach. *Phys. Chem. Chem. Phys.* **2019**, *21*, 18850−18865.

(11) Xue, K.; Sarkar, R.; Motz, C.; Asami, S.; Decker, V.; Wegner, S.; Tosner, Z.; Reif, B. Magic-Angle Spinning Frequencies beyond 300 kHz Are Necessary To Yield Maximum Sensitivity in Selectively

Methyl Protonated Protein Samples in Solid-State NMR. *J. Phys. Chem. C* **2018**, *122*, 16437−16442.
(12) Xue, K.; Sarkar, R.; Tosner, Z.; Lalli, D.; Motz, C.; Koch, B.; Pintacuda, G.; Reif, B. MAS dependent sensitivity of different isotopomers in selectively methyl protonated protein samples in solid state NMR. *J. Biomol. NMR* **2019**, *73*, 625−631.
(13) Penzel, S.; Oss, A.; Org, M.-L.; Samoson, A.; Böckmann, A.; Ernst, M.; Meier, B. H. Spinning faster: protein NMR at MAS frequencies up to 126 kHz. *J. Biomol. NMR* **2019**, *73*, 19−29.
(14) Xue, K.; Sarkar, R.; Motz, C.; Asami, S.; Camargo, D. C. R.; Decker, V.; Wegner, S.; Tosner, Z.; Reif, B. Limits of Resolution and Sensitivity of Proton Detected MAS Solid-State NMR Experiments at 111 kHz in Deuterated and Protonated Proteins. *Sci. Rep.* **2017**, *7*, 7444.
(15) Linser, R.; Bardiaux, B.; Andreas, L. B.; Hyberts, S. G.; Morris, V. K.; Pintacuda, G.; Sunde, M.; Kwan, A. H.; Wagner, G. Solid-State NMR Structure Determination from Diagonal-Compensated, Sparsely Nonuniform-Sampled 4D Proton−Proton Restraints. *J. Am. Chem. Soc.* **2014**, *136*, 11002−11010.
(16) Vasa, S. K.; Rovó, P.; Linser, R. Protons as Versatile Reporters in Solid-State NMR Spectroscopy. *Acc. Chem. Res.* **2018**, *51*, 1386−1395.
(17) Kurauskas, V.; Crublet, E.; Macek, P.; Kerfah, R.; Gauto, D. F.; Boisbouvier, J.; Schanda, P. Sensitive proton-detected solid-state NMR spectroscopy of large proteins with selective CH3 labelling: application to the 50S ribosome subunit. *Chem. Commun.* **2016**, *52*, 9558−9561.
(18) Chen, P.; Albert, B. J.; Gao, C.; Alaniva, N.; Price, L. E.; Scott, F. J.; Saliba, E. P.; Sesti, E. L.; Judge, P. T.; Fisher, E. W.; Barnes, A. B. Magic angle spinning spheres. *Sci. Adv.* **2018**, *4*, No. eaau1540.
(19) Agarwal, V.; Penzel, S.; Szekely, K.; Cadalbert, R.; Testori, E.; Oss, A.; Past, J.; Samoson, A.; Ernst, M.; Böckmann, A.; Meier, B. H. De Novo 3D Structure Determination from Sub-milligram Protein Samples by Solid-State 100 kHz MAS NMR Spectroscopy. *Angew. Chem., Int. Ed.* **2014**, *53*, 12253−12256.
(20) Hoult, D. I.; Richards, R. E. The signal-to-noise ratio of the nuclear magnetic resonance experiment. *J. Magn. Reson.* **2011**, *213*, 329−343.
(21) Reif, B.; Griffin, R. G. 1H detected 1H,15N correlation spectroscopy in rotating solids. *J. Magn. Reson.* **2003**, *160*, 78−83.
(22) Samoson, A. H-MAS. *J. Magn. Reson.* **2019**, *306*, 167−172.
(23) Tošner, Z.; Sarkar, R.; Becker-Baldus, J.; Glaubitz, C.; Wegner, S.; Engelke, F.; Glaser, SJ; Reif, B. Overcoming Volume Selectivity of Dipolar Recoupling in Biological Solid-State NMR Spectroscopy. *Angew. Chem., Int. Ed.* **2018**, *57*, 14514−14518.
(24) Hoult, D. I. The NMR receiver: A description and analysis of design. *Prog. Nucl. Magn. Reson. Spectrosc.* **1978**, *12*, 41−77.
(25) Zorin, V. E.; Brown, S. P.; Hodgkinson, P. Origins of linewidth in 1H magic-angle spinning NMR. *J. Chem. Phys.* **2006**, *125*, 144508.
(26) Penzel, S.; Smith, A. A.; Agarwal, V.; Hunkeler, A.; Org, M.-L.; Samoson, A.; Böckmann, A.; Ernst, M.; Meier, B. H. Protein resonance assignment at MAS frequencies approaching 100 kHz: a quantitative comparison of J-coupling and dipolar-coupling-based transfer methods. *J. Biomol. NMR* **2015**, *63*, 165−186.
(27) Bak, M.; Rasmussen, J. T.; Nielsen, N. C. SIMPSON: A General Simulation Program for Solid-State NMR Spectroscopy. *J. Magn. Reson.* **2000**, *147*, 296−330.
(28) Tošner, Z.; Andersen, R.; Stevensson, B.; Edén, M.; Nielsen, N. C.; Vosegaard, T. Computer-intensive simulation of solid-state NMR experiments using SIMPSON. *J. Magn. Reson.* **2014**, *246*, 79−93.
(29) Chevelkov, V.; Faelber, K.; Schrey, A.; Rehbein, K.; Diehl, A.; Reif, B. Differential Line Broadening in MAS solid-state NMR due to Dynamic Interference. *J. Am. Chem. Soc.* **2007**, *129*, 10195−10200.
(30) Asami, S. *Method Development for Biomolecular Solid-State NMR Spectroscopy*; Humboldt-Universität zu Berlin, Mathematisch-Naturwissenschaftliche Fakultät I, 2014.
(31) Agarwal, V.; Xue, Y.; Reif, B.; Skrynnikov, N. R. Protein side-chain dynamics as observed by solution- and solid-state NMR: a similarity revealed. *J. Am. Chem. Soc.* **2008**, *130*, 16611−16621.

https://dx.doi.org/10.1021/acs.jpcc.0c05407
J. Phys. Chem. C XXXX, XXX, XXX−XXX